Title

III-V COMPOUND SUBSTRATE AND EPITAXIAL LAYER CHARACTERIZATION BY DIVERGENT X-RAY BEAM DIFFRACTION

Authors

Donaghey, L.F.
Bissinger, R.H.

Publication Date

1973-07-01

Submitted to Journal of
Electronic Materials

LBL-1872
Preprint

III-V COMPOUND SUBSTRATE AND EPITAXIAL LAYER CHARACTERIZATION BY DIVERGENT X-RAY BEAM DIFFRACTION

L. F. Donaghey and R. H. Bissinger

July 1973

Prepared for the U. S. Atomic Energy Commission
under Contract W-7405-ENG-48

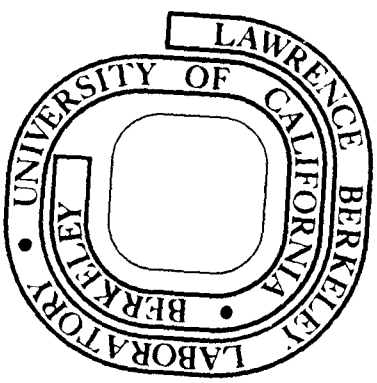

LBL-1872

DISCLAIMER

III-V Compound Substrate and Epitaxial Layer Characterization by Divergent X-ray Beam Diffraction

L. F. Donaghey and R. H. Bissinger

Inorganic Materials Research Division of the
Lawrence Berkeley Laboratory and the
Department of Chemical Engineering of the
University of California
Berkeley, California 94720

Abstract

The divergent x-ray beam diffraction method was studied for the characterization of lattice perfection in GaAs substrates and of composition variation and growth defects in epitaxial $GaAs_{1-x}P_x$ layers. Reflections from the $\{7\bar{1}1\}$, $\{620\}$, $\{551\}$ and (400) planes predominate in pseudo-Kossel back reflection patterns obtained from samples with (100) surface orientations. The selectivity of pseudo-Kossel line displacements is assessed for lattice parameter and anisotropic strain distortion measurement. Lattice parameter variations in epitaxial layers are accurately measurable from $\{551\}$, $\{444\}$ and $\{422\}$ plane reflections, while (400) line displacements can be used to measure lattice strain.

Introduction

The divergent beam x-ray diffraction method offers considerable potential in the analysis of crystallographic and microstructural properties of epitaxial single crystal layers. The divergent beam method, originally developed by Imura[1,2] for the study of deformation and lattice defects in single crystals, allows with high precision the measurement of the lattice parameters and orientation of single crystals.[3] This method can also yield information on lattice parameter variations, as well as on lattice distortion and can yield topographical mapping of lineage substructure in graded epitaxial layers.

Although the epitaxy of deposited films on single crystal surfaces has been studied by many methods, Wood was the first to apply the divergent beam x-ray diffraction method to observe the orientation of epitaxial films produced by electrodeposition on well characterized substrates.[4] More recently, Lighty applied the method to the study of electrodeposited epitaxial copper films.[5] The application of this method of x-ray diffraction to characterize lattice properties of III-V compound substrates and epitaxial layers of semiconducting materials has not been previously reported.

In this paper the potential applicability of this method to the characterization of lattice perfection in single crystal substrates and of growth defects in epitaxial, graded composition layers of III-V compounds is examined. The calculations are confined to the diffraction of $CuK_{\alpha 1}$ x-radiation from GaAs, but the methods apply equally to other III-V compounds and alloys.

Pseudo-Kossel Line Generation

The apparatus for back reflection x-ray diffraction of divergent beams is shown schematically in Fig. 1. The divergent x-ray beam is generated by electrostatically focussing high energy electrons onto the center of a thin metal foil target. If the electron accelerating voltage is sufficiently high, characteristic x-radiation emerges from the foil in all directions. The radiation emerging from the vacuum side of the target foil is absorbed by the electron beam tube while that emerging from the opposite side irradiates a bulk sample placed from 0.1 to 1 cm in front of the point x-ray source.

X-ray diffraction from crystallographic sets of planes in the specimen produce both forward and back-reflection patterns which Imura et al.[1] have termed pseudo-Kossel patterns. Whereas true Kossel patterns are produced by diffraction of a point source of characteristic x-rays generated on the sample surface by a focussed electron beam,[7] the x-ray point source

for pseudo-Kossel patterns produces non-characteristic x-radiation generated at a point removed from the sample surface. The Kossel diffraction envelopes are true cones, but the pseudo-Kossel diffraction lines are conics distorted by reflection from the sample surface. These distorted cones intersect the photographic film in ellipses which are symmetric about their major axes, but which have minor axes displaced toward the beam axis. Each ellipse in the pattern originates by diffraction from a different set of (hkl) planes.

As an example of the diffraction geometry, Fig. 1 shows x-ray diffraction of $CuK_{\alpha 1}$ x-rays from (hkl) planes inclined at an angle β from the sample surface. The plane of the drawing thus contains the surface normal $\vec{n}_{HKL}$ and the (hkl) plane normal $\vec{n}_{hkl}$. Since diffraction occurs only at the Bragg angle, the back-diffracted beam will intersect the film on the axis shown, with the beam axis as origin, at y_2 and y_2'. The camera dimensions a and b both adjust the size of the ellipse major axes, with b limited by the available sample size so as to produce diffraction at y_1 and y_1', and with the length a limited by the film size for recording a given pseudo-Kossel ellipse.

Differences in (hkl) plane orientations and spacing produce measurable displacements in pseudo-Kossel line positions. For example, a displacement in the camera distance, Δb, produces displacements Δy_2 and $\Delta y_2'$ in line positions along the major axis. The relationship between the observed line

displacements Δy_2 and the sample displacement Δb provides the basis for lattice parameters determination once the pseudo-Kossel lines are indexed. Lattice distortion and epitaxial growth defects produce similar displacements Δy_2.

Pseudo-Kossel Pattern Indexing

The interpretation of pseudo-Kossel patterns produced by back reflection of a divergent x-ray beam is relatively simple for samples with planar surfaces of known orientation. The direction and extent of pseudo-Kossel ellipses can then be deduced from geometrical constructions involving the Bragg angle, θ, and the inclination angle β between the diffracting planes and the sample surface, as shown in Fig. 1.

The diffraction parameters required in the calculation of pseudo-Kossel patterns produced by divergent beam back reflection from (100) GaAs are summarized in Table 1. The Bragg diffraction angle θ is tabulated for each plane, as are the plane-inclination angles β. Only those diffracting planes yielding finite diffraction intensities for $CuK_{\alpha 1}$ x-radiation are listed. Since only those planes for which $\theta-\beta > 0$ and $\theta+\beta < 180°$ will produce back reflected x-rays, not all $\{hkl\}$ planes will contribute to the back reflection pattern. The β angles of planes contributing to forward diffraction are therefore listed in parentheses.

The maximum and minimum radii of pseudo-Kossel lines can now be calculated from the tabulated data and from the conditions of Fig. 1. The line coordinates on the sample surface and photographic film along the major axis are related to the film-target and target-sample distances a and b, respectively, by the relations,

$$\begin{aligned} y_1 &= b \cot(\theta+\beta) \\ y_2 &= b \cot(\theta+\beta) + (a+b) \cot(\theta-\beta) \\ y_1' &= -b \cot(\theta-\beta) \\ y_2' &= -b \cot(\theta-\beta) - (a+b) \cot(\theta+\beta) \end{aligned} \tag{1}$$

For (100) GaAs and CuK_α x-radiation the superpositions of the diffraction rays for all planes containing the beam axis and (hkl) plane normals is shown in Fig. 2 for camera distances a and b equal to 3 and 1 units, respectively. This figure allows the prediction of pseudo-Kossel line major axis-intercepts y_2 and y_2' for all camera constants a and b by the following construction: the constant b is taken as the unit distance and an arbitrary film plane is drawn perpendicular to the electron beam axis such that the film-target distance a is the desired number of unit distances; the hkl plane diffracted rays will then intercept the new film plane at distances y_2 and y_2' measured on the diagram in unit distances from the beam axis.

The sample size required to produce diffraction from a given set of lattice planes for a fixed target-sample distance

can also be determined with the aid of Fig. 2. The figure indicates (200) and {444} reflections occur at the largest distances from the electron beam axis. Samples of limited cross-section can be examined by the divergent beam diffraction method provided that the target-sample distance is sufficiently reduced. For larger target-sample distances these reflections are permitted only with special sample placement.

A similar construction can be made to calculate the minor axis end points of pseudo-Kossel ellipses. This is done by constructing the plane perpendicular to the plane of Fig. 1, but which contains the (hkl) plane normal and passes through the x-ray point source. Sample and film coordinates of pseudo-Kossel lines in this plane are then

$$\begin{aligned} x_1 &= -x_1' = b \cot\theta \sec\beta \\ x_2 &= -x_2' = (a+2b) \cot\theta \sec\beta \end{aligned} \qquad (2)$$

where the x-axis lies in the film plane perpendicular to the y-axis shown in Fig. 1.

The major and minor axis dimensions of complete ellipses in the back-reflection pseudo-Kossel pattern are useful for indexing the ellipses in terms of diffracting planes, provided that the camera dimensions a and b are known. In terms of the parameters of Fig. 1 it can be shown that the ellipse major axis diameter, y_2-y_2', is given by

$$\text{Major axis diameter} = (a+2b)[\cot(\theta+\beta) + \cot(\theta-\beta)] \qquad (3)$$

Similarly, the minor axis diameter, x_2-x_2', is

$$\text{Minor axis diameter} = 2(a+2b)\ \sec\beta\ \cot\theta \tag{4}$$

Note that the ellipses are asymmetrically distorted toward the beam axis and thus it is necessary to take the largest dimension perpendicular to the major axis as the minor axis diameter. If the reduced variables

$$v = \frac{2(a+2b)}{y_2-y_2'}$$
$$u = \frac{2(a+2b)}{x_2-x_2'} \tag{5}$$

are defined, then the (100) to (hkl) interplanar angle β can be found from the root of the equation,

$$\cos^3\beta + (u^2-1)\cos\beta = uv \tag{6}$$

Similarly, the Bragg angle θ can be deduced from the equation,

$$\cot^3\theta + (1-u^{-2})\cot\theta = vu^{-2} \tag{7}$$

The Miller indices of the diffracting plane are then calculable from Bragg's law and from the inter-planar angle formula. As an example, for samples with (100) surface orientations, the Miller indices are

$$h = 2a_o\lambda^{-1}\sin\theta\cos\beta$$
$$k^2+l^2 = (2a_o\lambda^{-1})\sin\theta\sin\beta \tag{8}$$

The final distinction between the Miller indices k and l requires

a stereographic projection of possible diffracting planes for the zinc blende structure.

The symmetry of equivalent {hkl} diffracting planes about the electron beam axis provides a simple basis for indexing pseudo-Kossel pattern ellipses. The stereographic projection of {hkl} plane normals onto the (100) plane in the zinc blende structure is shown in Fig. 3a. Ellipse indexing is achieved by superimposing the stereogram onto the pseudo-Kossel pattern so that vectors from the stereogram center to {hkl} projections lie along ellipse major diameters. Each ellipse is assigned the corresponding hkl index. From such a projection one can expect {lln} plane diffractions to produce ellipses appearing in sets of four oriented at 45°, 135°, 225° and 315° from the [010], while eight-fold additional ellipses are generated by diffraction from {nll} planes and appear in pairs oriented symmetrically about ⟨100⟩ directions. The latter set cannot be distinguished from {nnl} plane ellipses, however, and cause ambiguous ellipse assignments if they are made by symmetry arguments alone.

The ambiguity in ellipse assignments is lifted if only those planes with normals within 45° of the beam axis are included in the stereogram. Fig. 3b shows the (100) stereographic projection of {hkl} planes which produce pseudo-Kossel pattern ellipses by back-diffraction of $CuK_{\alpha 1}$ x-radiation (λ = 1.54051 Å) from (100) GaAs. All diffracting planes contributing to the back-reflection pattern are inside the

45° central zone of the stereogram for this case. Additional {hkl} plane reflection diffractions outside the 45° central zone are possible for samples with smaller lattice parameters and for x-ray targets producing longer wavelengths, but the additional ellipses usually lie far from the central region of the back-diffraction pattern.

The fully indexed pseudo-Kossel pattern obtained by back reflection diffraction from (100) GaAs is shown in Fig. 4. The most prominent lines are the four-fold {117} and {026}, the eight-fold {155} and the single (400) plane reflections.

Lattice Parameter and Strain Measurement

The application of the divergent x-ray beam diffraction method to structural analysis requires conditions that favor a high selectivity of pseudo-Kossel line positions to crystallographic properties of the sample lattice. In this section the selectivity of back reflection pattern lines is examined for lattice parameter and anisotropic lattice distortion determination.

The Film Displacement Method

Crystal lattice parameter determination by the divergent x-ray beam method has been discussed by Ellis et al.[3] These authors eliminate errors in the measurement of camera constants a and b by taking multiple exposures after successive displacements of the film plane. The measured displacements in the

(hkl) pseudo-Kossel line positions along the major axis are related to the film plane displacement Δa by

$$\begin{aligned} \Delta y_2 &= \Delta a \cot(\theta-\beta) \\ -\Delta y_2' &= \Delta a \cot(\theta+\beta) \end{aligned} \tag{9}$$

The lattice parameter can then be calculated from

$$a_o = \frac{1}{2}\lambda \sqrt{h^2+k^2+l^2} \sin\left\{\frac{1}{2}\left[\cot^{-1}\left(\frac{\Delta y_2}{\Delta a}\right) + \cot^{-1}\left(\frac{-\Delta y_2}{\Delta a}\right)\right]\right\} \tag{10}$$

The sensitivity of the method can be assessed by considering a differential displacement in y_2 produced by an incremental film plane displacement da,

$$\frac{\partial y_2}{\partial a} = \cot(\theta-\beta)$$

The magnitudes of this differential for (hkl) pseudo-Kossel lines from GaAs are shown in Table II. The {422}, (200) and {444} lines yield the highest sensitivity, but the diffracted beam intensities are low and the ellipses often are incomplete. Since the above method for lattice parameter determination requires complete pseudo-Kossel ellipses for the measurement of $\Delta y_2'$, the {444} reflections cannot be used since y_2' falls within the central hole in the film plane required to pass the electron beam tube.

The Sample Displacement Method

An alternate method for lattice parameter measurement is proposed here in which the displacements in pseudo-Kossel lines are measured for a precise sample displacement as shown in Fig. 1. A sample displacement Δb will then produce (hkl) line displacements along ellipse major axes of amounts

$$\begin{aligned} \Delta y_2 &= \Delta b \cot\left[(\theta-\beta) + \cot(\theta+\beta)\right] \\ -\Delta y_2 &= \Delta b \cot\left[(\theta-\beta) + \cot(\theta+\beta)\right] \end{aligned} \tag{11}$$

The displacements Δy_2 and $-\Delta y_2$ are identical and, therefore, only Δy_2 needs to be measured. This method requires that the sample surface orientation be known, from which the (hkl) plane inclination angle β can be calculated.

The sensitivity of pseudo-Kossel line displacements produced by an incremental sample displacement is then

$$\frac{\partial y_2}{\partial b} = \cot(\theta+\beta) + \cot(\theta-\beta) \tag{12}$$

Table II summarized the magnitude of this differential for different (hkl) plane reflections from GaAs. Line displacement sensitivities for sample displacements are comparable to but generally larger than those for film plane displacement. The sample displacement method offers greater selectivity for certain pattern lines and is easier to carry out for those ellipses passing near the beam axis.

Epitaxial Film Lattice Parameter Measurement

Differences in lattice parameters between the substrate and a thin epitaxial layer can be deduced directly from pseudo-Kossel patterns since the pseudo-Kossel line positions are strong functions of lattice plane spacing. From Eq. 1 and Bragg's law one finds that the variation of a line position y_2 with lattice parameter a_o is given by

$$\frac{\partial y_2}{\partial a_o} = a_o^{-1} \tan\theta \left[b \csc^2(\theta+\beta) + (a+b) \csc^2(\theta-\beta) \right] \qquad (14)$$

The resolution between substrate and epitaxial layers is increased if the lattice parameter of the epitaxial layer is smaller than that of the substrate, whereas the two sets of diffraction lines tend to overlap when the lattice parameter decreases with increasing depth.

The product $a_o \partial y_2 / \partial a_o$ is tabulated in Table II for (hkl) plane diffractions from GaAs, showing that highest precision can be obtained with the $\{422\}$ and $\{444\}$ plane reflections. As the latter line intensities are low, however, the measurements from $\{551\}$ plane reflections are recommended for lattice parameter measurements in epitaxial layers.

Strain Measurements

A strain analysis using the divergent beam method was recently developed by Imura et al.[2] who calculated the principal strain in a crystal from measured changes in interatomic spacings of more than six independent (hkl) reflections.

The change in interatomic spacings Δd_{hkl} induced by mechanical stress is indistinguishable from the corresponding change Δd_{hkl} induced by chemical composition changes. Thus, for chemically pure samples the pseudo-Kossel line displacement sensitivities to lattice parameter, as described in the preceding section, form the basis for a principal strain analysis.

In epitaxial layers containing growth defects[6,7] the displacements in (hkl) plane orientation are expected to be larger than displacements in interplanar spacing. The orientational change for a set of (hkl) planes is of two types. A uniform orientational change within a microcrystalline region is called homogeneous strain or macrostrain, whereas a broadening of the diffraction line due to a continuous variation in (hkl) plane spacing is called inhomogeneous strain broadening or microstrain. The line profile theory of Warren[8] and the inhomogeneous strain and coherency domain size determination method developed by Warren and Auerbach[9] are the basis for line broadening analysis. Microstrain and orientational change analysis is difficult because each pseudo-Kossel line is produced by diffraction from a different region of the sample.

The sensitivity of pseudo-Kossel line displacements induced by a differential change in the (hkl) plane inclination angle β is found from Eq. 1 to be

$$\frac{\partial y_2}{\partial \beta} = b \csc^2(\theta-\beta) - (a+b) \csc^2(\theta+\beta) \qquad (15)$$

The magnitudes of this differential for different (hkl) planes are also shown in Table II. The (200) and {422} plane reflections provide the most sensitive measurement of (hkl) plane orientational change. Of the most prominent lines in the pseudo-Kossel pattern, however, the (400) reflection provides the highest sensitivity.

Conclusions

The divergent x-ray beam method is a promising analytical technique for characterizing the lattice perfection of substrate crystals and growth defects in epitaxial layers. The pseudo-Kossel patterns generated for (100) orientation III-V compounds are easily indexed in terms of the Bragg angle for diffraction and interplanar angles. The selectivity of pseudo-Kossel line displacements induced by film and sample positions and by lattice parameter and (hkl) plane orientational changes were assessed for GaAs. The {444}, {551} and (400) plane reflections gives greatest sensitivity for lattice parameter measurements by the sample displacement method and give highest sensitivity for measurement of inhomogeneous and homogeneous strain. Of the most prominent lines in the (100) pseudo-Kossel pattern for GaAs the {551} lines show the largest sensitivity to lattice parameter differences between epitaxial layer and substrate.

Acknowledgment

This work was performed under the auspices of the U. S. Atomic Energy Commission.

References

1. T. Imura, J. Appl. Inst. Metals 16, 10 (1952); Naniwa Univ. Ser. 2, 51 (1954); Bull. Univ. of Osaka Prefecture, Ser. A 5, 1 (1957).
2. T. Imura, S. Weissman and J. J. Slade, Jr., Acta Crystallographica 8, 786 (1962).
3. T. Ellis, L. F. Nanni, A. Shrier, S. Weissman, G. E. Padawer and N. Hosokawa, J. Appl. Phys. 35, 3364 (1964).
4. W. A. Wood, Proc. Phys. Soc. (London) 43, 138 (1931).
5. P. E. Lighty, D. Shanefield, S. Weissman and A. Shrier, J. Appl. Phys. 34, 2233 (1963).
6. E. T. Peters and R. E. Ogilvie, Trans. Met. Soc. AIME 233, 89 (1965).
7. D. B. Holt, J. Phys. Chem. Solids 27, 1053 (1966).
8. M. S. Abrahams, L. R. Weisberg, C. J. Buicocchi and J. Blanc, J. Mat. Science 4, 223 (1969).
9. B. E. Warren, Prog. Metal Phys. 8, 147 (1959).
10. B. E. Warren and B. L. Averbach, J. Appl. Phys. 21, 595 (1950).

Table I

Diffraction Parameters for Back-Reflection Pseudo-Kossel Patterns from (100) GaAs

hkl	I/I_Q	d(Å) (1)	θ (deg) (2)	β (deg) (3)			θ+β	θ-β	cot(θ+β)	cot(θ-β)
111	100	3.26409	13.649	(54.736) (4)			-	-	-	-
200	1	2.82670	15.812	0.000	(90.000)		15.812	15.812	3.5311	3.5311
220	35	1.99880	22.666	(45.000)	(90.000)		-	-	-	-
311	35	1.70458	26.864	25.239	(72.452)		52.103	1.625	0.7784	35.2495
400	6	1.41335	33.023	0.000	(90.000)		33.023	33.023	1.5385	1.5385
331	8	1.29698	36.433	(46.508)	(76.737)		-	-	-	-
422	6	1.15399	41.872	35.264	(65.905)		77.136	9.805	0.2284	5.7864
333	4	1.08799	45.069	(54.736)			-	-	-	-
511	4	1.08799	45.069	15.793	(78.904)		60.862	29.276	0.5575	1.7837
440	2	0.99940	50.418	45.000	(90.000)		95.418	5.418	-.0948	10.544
531	2	0.95560	53.711	32.312	(59.530)	(80.268)	86.023	21.399	0.0695	2.5518
620	4	0.89387	59.508	18.435	(71.565)	(90.000)	77.943	41.073	0.2136	1.1474
533	2	0.86214	63.306	40.316	62.774 (5)		103.622	22.990	-.2423	2.3570
444	4	0.81600	70.723	54.736			125.459	15.987	-.7122	3.4904
711	2	0.79133	76.651	11.422	(81.951)		88.073	65.229	0.0336	0.4614
551	2	0.79133	76.651	45.562	(81.951)		122.213	31.089	-.6300	1.6584

(1) $d = a_o/\sqrt{h^2+k^2+l^2}$, a_o = 5.6534 Å for GaAs

(2) $\theta = \sin^{-1}[\lambda/(2d)]$, λ = 1.54051 Å for $CuK_{\alpha 1}$ x-radiation

(3) $\beta = \cos^{-1}(Hh+Kk+Ll) / \sqrt{(H^2+K^2+L^2)(h^2+k^2+l^2)}$, (HKL) = (001)

(4) Interplanar angles shown in parentheses correspond to transmission diffraction.

(5) θ±β values are omitted.

Table II.

Differential displacements of the pseudo-Kossel line parameter y_2 for camera lengths a = 3 cm and b = 1 cm

hkl	$\frac{\partial y_2}{\partial a}$	$\frac{\partial y_2}{\partial b}$	$\frac{\partial y_2}{\partial \beta}$	$a_o \frac{\partial y_2}{\partial a_o}$
200[1]	3.5311	7.0622	19.072	-40.4060
400	1.5385	3.0770	10.9428	-10.0994
422[1]	5.7864	6.0148	31.8515	30.2735
511	1.7837	2.3412	5.5056	- 1.0614
531	2.5518	2.6213	11.5987	3.4925
620	1.1474	1.3610	5.7096	- 1.8659
533	2.3570	2.1147	15.1428	2.3205
444	3.4904	2.7782	42.0036	7.1539
711	0.4614	0.4950	9.3308	- 2.7916
551	1.6584	1.0284	21.6927	- 1.8374

[1] Large sample area or special film placement required.

List of Figures

Fig. 1: Camera geometry for back-reflection pseudo-Kossel x-ray diffraction patterns in the plane containing the beam axis and the diffracting plane normal.

Fig. 2: Back-reflection diffraction of $CuK_{\alpha 1}$ x-radiation from (hkl) planes of GaAs, for film-target and target-sample distances of 3 and 1 cm, respectively. The figure shows superpositions of diffraction in planes containing the (hkl) plane normals.

Fig. 3a: Stereographic projection of {hkl} poles onto the (100) plane of the zinc blende structure.

Fig. 3b: Stereographic projection of {hkl} poles contributing to back-reflection pseudo-Kossel lines from (100) GaAs.

Fig. 4: Pseudo-Kossel pattern for (100) GaAs produced by back-reflection diffraction of $CuK_{\alpha 1}$ x-radiation with camera constants a = 3.06 cm and b = 1.07 cm.

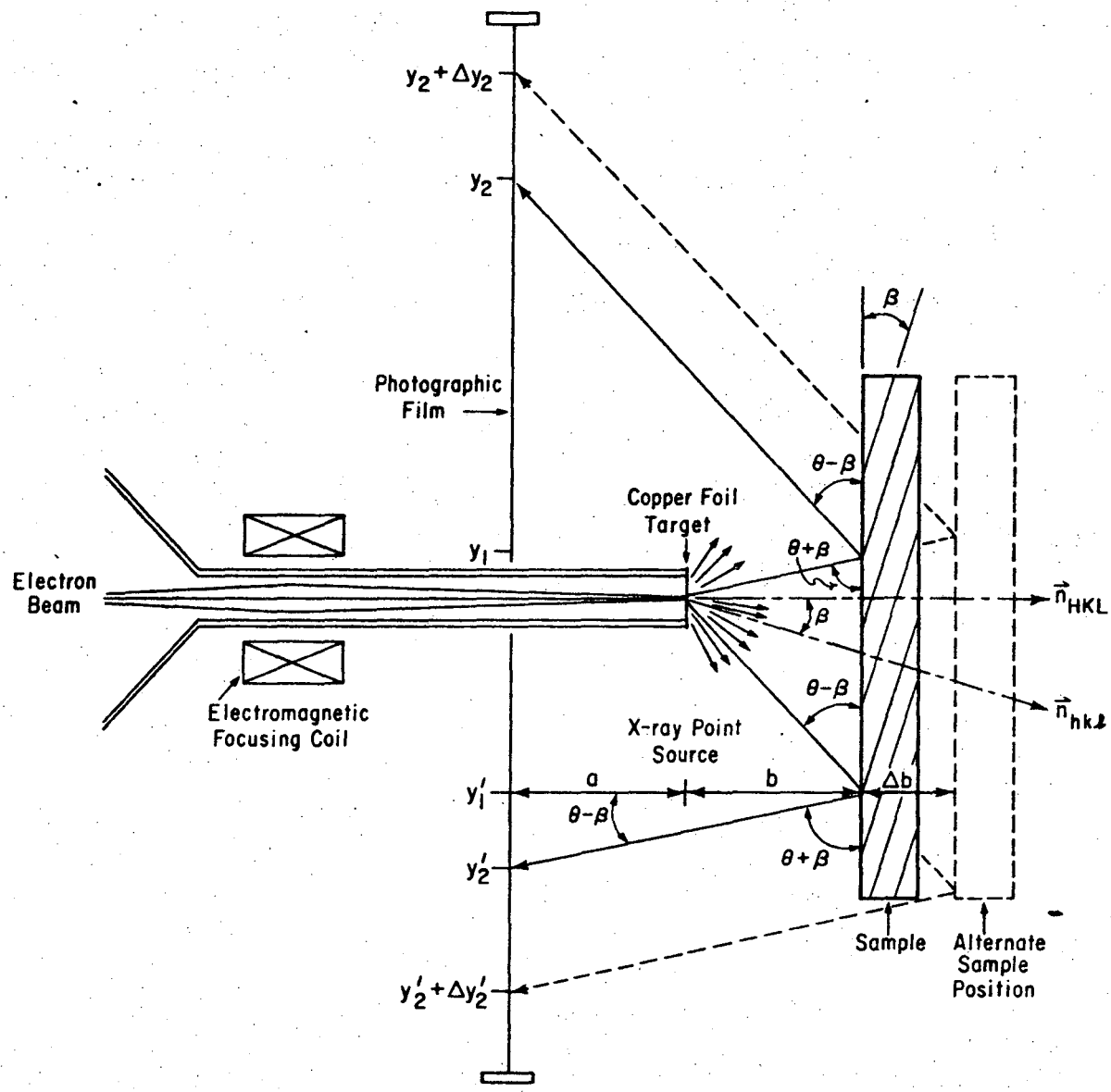
$y_2+\Delta y_2$
y_2
Photographic Film
y_1
Copper Foil Target
Electron Beam
Electromagnetic Focusing Coil
X-ray Point Source
y_1'
y_2'
$y_2'+\Delta y_2'$
a
b
Δb
β
$\theta-\beta$
$\theta+\beta$
$\vec{n}_{HKL}$
$\vec{n}_{hkl}$
Sample
Alternate Sample Position
XBL 737-6494

Fig. 1

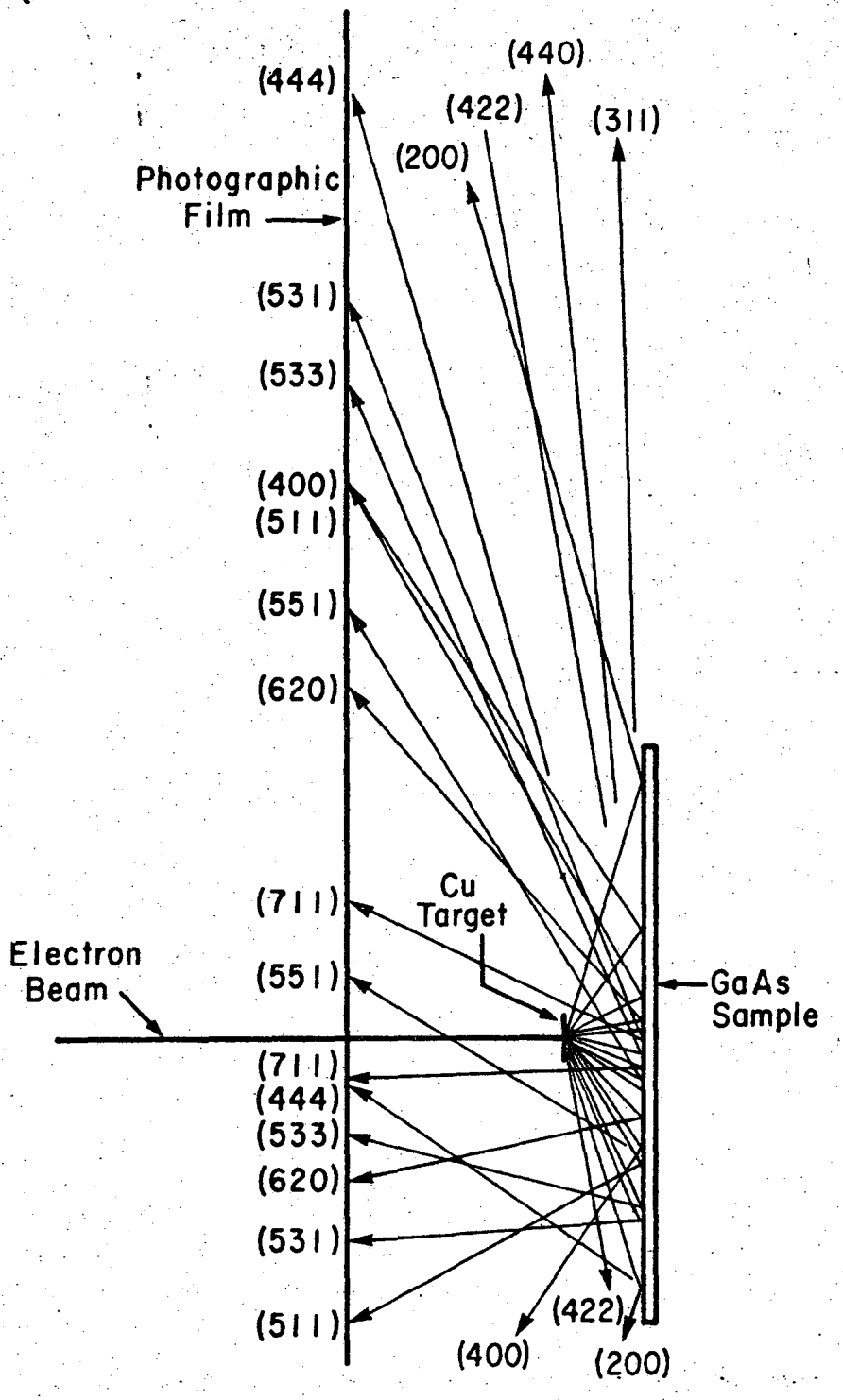

XBL 737-6495

Fig. 2

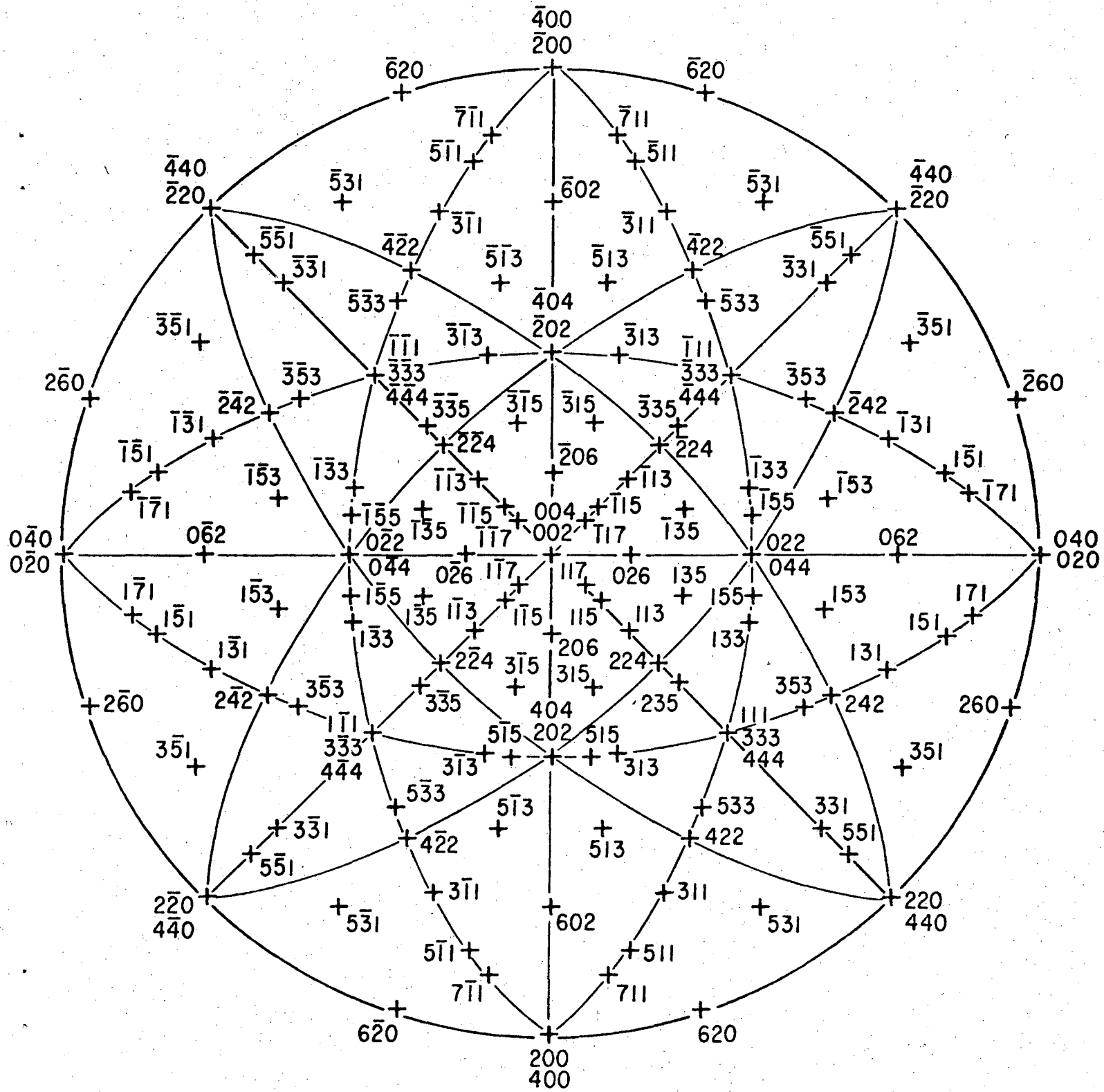

XBL 737-6496

Fig. 3a

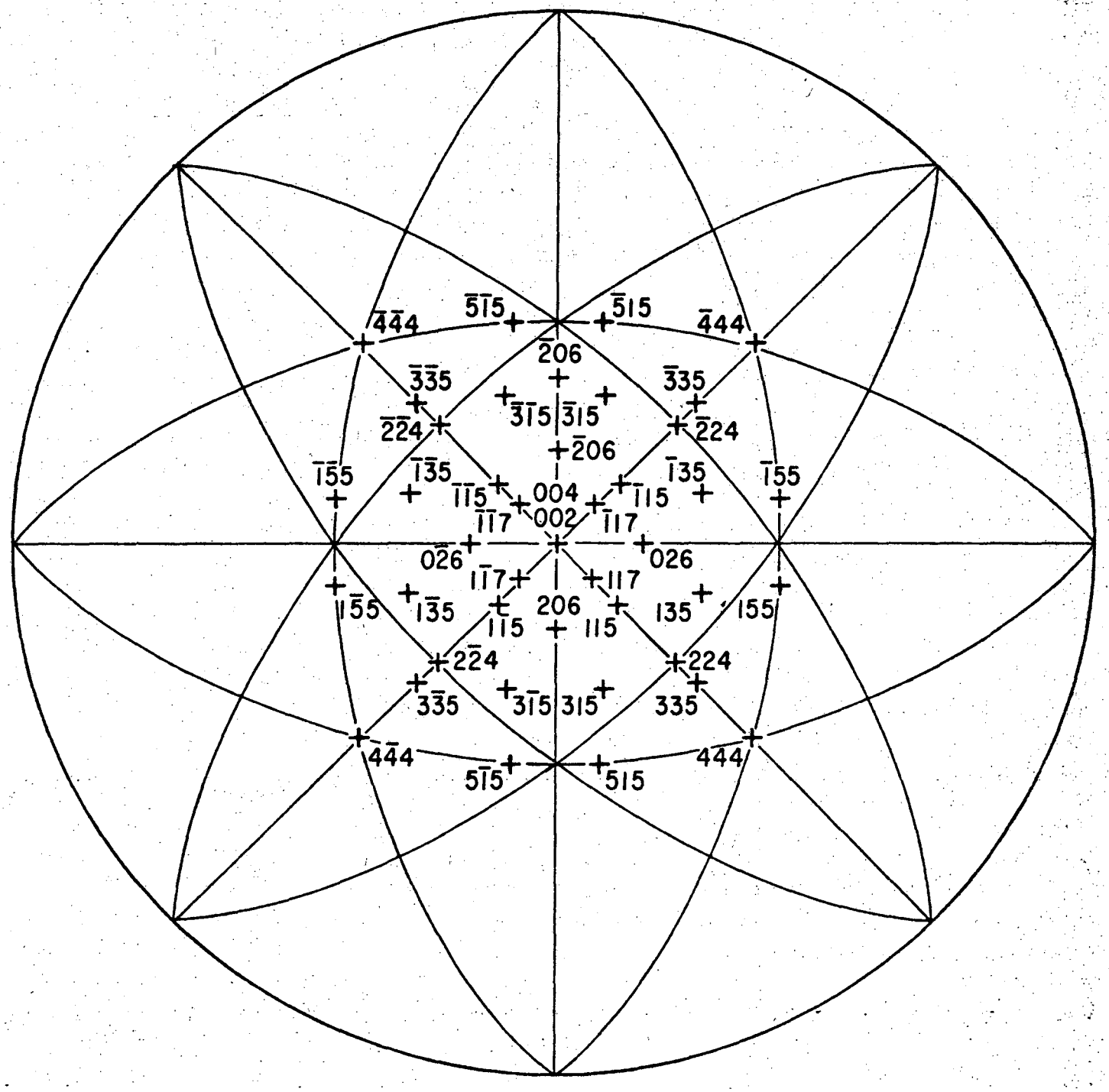

XBL 737-6497

Fig. 3b

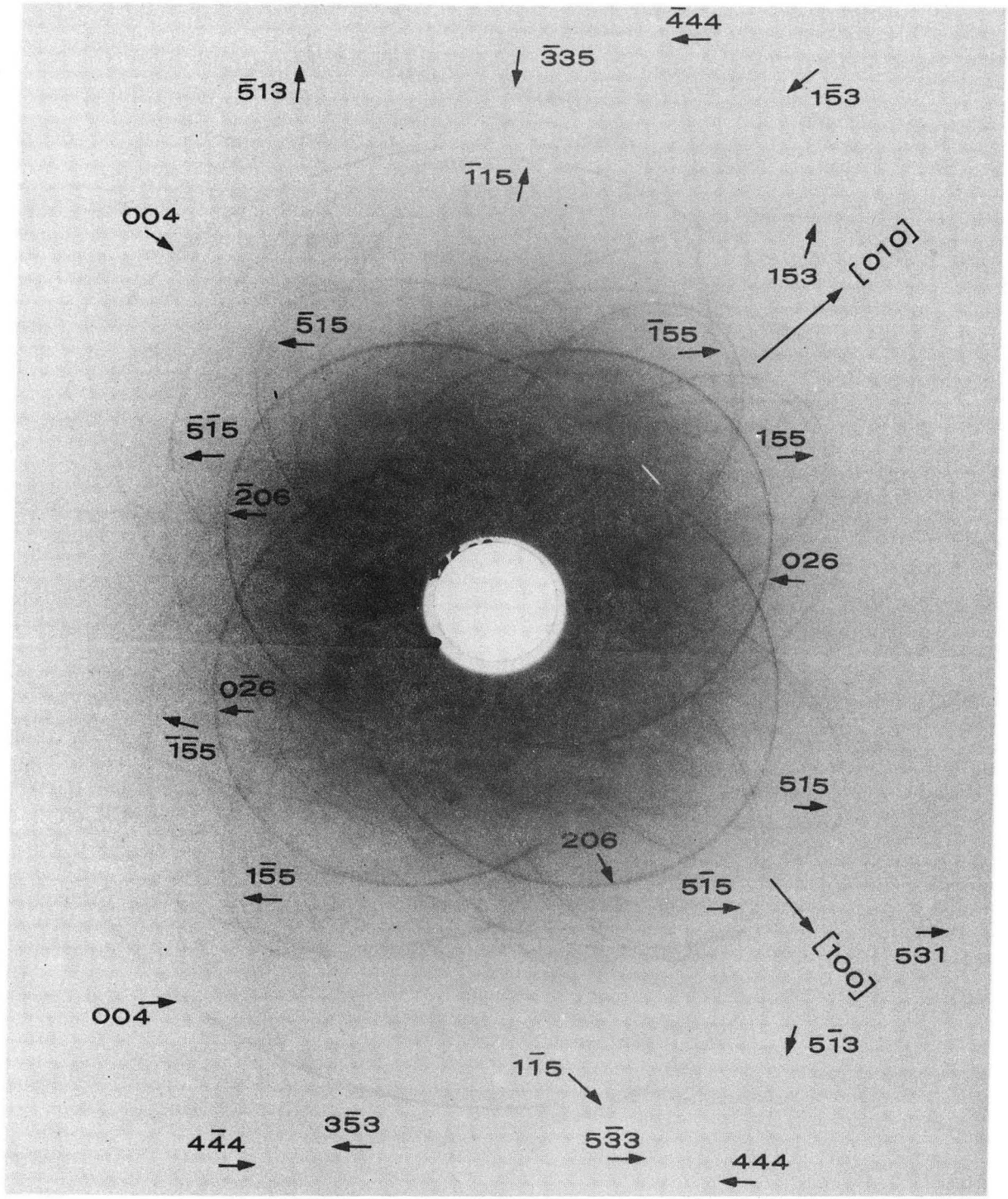

XBB 737-4370

Fig. 4

TECHNICAL INFORMATION DIVISION
LAWRENCE BERKELEY LABORATORY
UNIVERSITY OF CALIFORNIA
BERKELEY, CALIFORNIA 94720